

Carbon Nano-Flakes Produced by an Inductively Coupled Thermal Plasma System for Catalyst Applications

Ramona Pristavita · Jean-Luc Meunier · Dimitrios Berk

Received: 1 November 2010 / Accepted: 1 February 2011 / Published online: 16 February 2011
© Springer Science+Business Media, LLC 2011

Abstract Carbon material was produced using an inductively coupled thermal plasma torch system of 35 kW and a conical shape reactor. The carbon nanopowders were obtained by plasma decomposition of methane at various flow rates and show a uniform microstructure throughout the reactor. The product has a crystalline graphitic structure, with a stacking of between 6 and 16 planes and a nano-flake morphology with particles dimensions of approximately 100 nm long, 50 nm wide and 5 nm thick. Nitrogen was also introduced in some synthesis experiments along with the methane precursor using flow rates of 0.1 and 0.2 slpm. The resulting product has the same structural properties and the nitrogen is incorporated into the graphitic structure through pyridinic type bonds.

Keywords Carbon nano-flakes · Thermal plasma · Nitrogen functionalization · Graphitic structure

Introduction

Carbon presents different allotropic forms such as diamond, graphite, carbon nanotube structures, fullerene family based solids, and amorphous carbon. The carbon atoms in graphite are organized in the form of layers of symmetrical hexagons, each of these layers being horizontally displaced relative to the next one. Starting with this perfect crystalline arrangement, degenerated structures can be constructed based on lower degrees of symmetry down to a completely amorphous structure. From the physical point of view, carbon black (CB) is an intermediate structural form between graphite and an amorphous structure [1].

Industrially, CB is produced using two main types of manufacturing processes: the furnace process and the thermal process. The furnace process uses heavy aromatic oils as feedstock and a closed reactor to atomize this feedstock. The reaction rate is controlled by steam or water spraying. The thermal process uses natural gas as feedstock and a pair of

R. Pristavita (✉) · J.-L. Meunier · D. Berk
Department of Chemical Engineering, McGill University,
3610 University St., Montreal, QCH3A 2B2, Canada
e-mail: ramona.turcu@mail.mcgill.ca

furnaces that alternate approximately every 5 min between preheating and carbon black production.¹ More recently, plasma technologies have been used as a route for the synthesis of new CB structures [2–7]. One of the advantages of such a technology is the possibility to use a variety of carbon sources in gaseous, liquid or solid state. The plasma process is also clean, it does not generate CO₂ and the resulting CB powders do not contain large amounts of impurities as those found in the flame processes.

In a thermal plasma system, the particle size and the number of nucleated particles are affected by two factors: the cooling rate at the location of the nucleation and the monomer concentration. High monomer concentration and low cooling rates favor the nucleation of fewer particles having a larger particle size [3, 4]. The properties of the product are also influenced by the local temperature: injection of the carbon source in the arc zone ($T \sim 10,000$ K for argon plasma) results in production of a highly organized CB. The growth of the particles in a low temperature region of the reactor ($T < 1,600^\circ\text{C}$) will lead to an amorphous product with spherical particles [5]. The nature of the feedstock does not influence the size distribution of CB aggregated but an important role is played by the zone where the carbon source is injected [2].

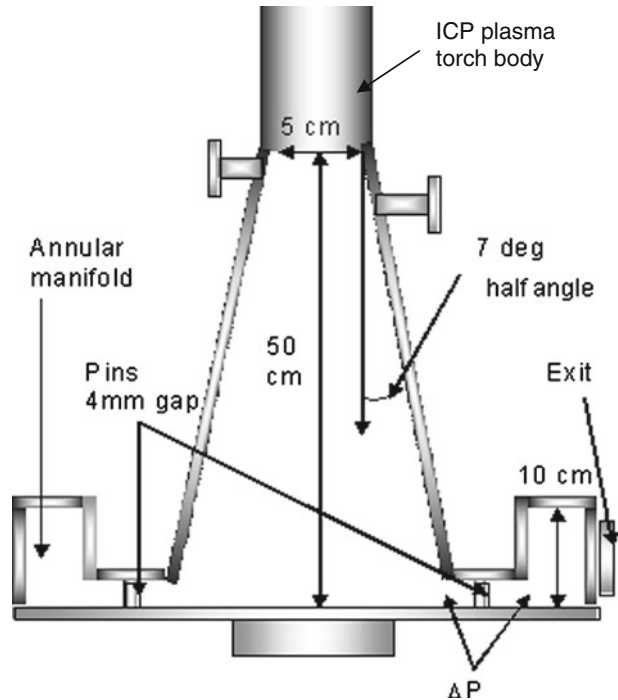
CB is widely used in industry, including in the energy and transportation sectors for example as a catalyst support in the Polymer Electrolyte Membrane (PEM) fuel cell. A typical carbon black material used in PEM fuel cell studies is Vulcan XC72R produced by Cabot, although other carbons such as Black Pearls, Ketjen Black or Printex XE-2 produced by Degussa have also been used [8–11]. The PEM fuel cells are clean and efficient alternative energy sources; however their production cost must be reduced substantially in order for them to be economically viable. Of particular importance in the cost reduction is the development of an alternative, low cost catalyst. The catalyst material used presently consists of CB powder on which fine platinum (Pt) particles are uniformly dispersed. CB was chosen because of its electrical conductivity, its high surface area and its ability to function in the highly acidic medium of the PEM fuel cells. Pt particles typically catalyze oxidation reaction taking place at the anode and the reduction reaction taking place at the cathode. While non-platinum catalysts still show lower activity and much lower durability than Pt, recent improvements in their beginning-of-life activity give increased hope for their eventual practicality [12]. The non-noble catalysts materials consist also of CB powder which contains nitrogen atoms bonded to the graphitic support and iron atoms bounded to the nitrogen atoms, creating in this way the active Fe centers for catalysis [13]. These active centers have a structure of metal-N₄ chelates. The metal atoms coordinated into the active site can be any transition metal, but iron and cobalt are known to present the highest electrocatalytic activities [14].

The results presented in this communication are part of an overall work whose objective is to produce and control the morphology of CB nanopowders having a high density of catalytic sites on their surface leading to a high catalytic activity. The active centers are formed inside the pores of the material or on the edge of the graphene planes. Thus the degree of crystallinity of the produced material and its porosity are two of the most important properties of such a catalyst material [11, 13]. In terms of the chemical structure, the increase in the number of catalytic sites requires not only a crystalline nanostructure of the powders but also an increase in the quantity of nitrogen incorporated in the nanostructure.

In this paper we present carbon nano-powders having a crystalline flake-like morphology which is obtained by plasma decomposition of methane at various flow rates in the

¹ Carbon Black User's Guide. Safety, Health, and Environmental Information. International carbon black association (ICBA) www.carbon-black.org.

Fig. 1 Diagram of conical water cooled reactor [12]



presence and absence of nitrogen using an inductively coupled thermal plasma (ICP) torch system.

Experimental

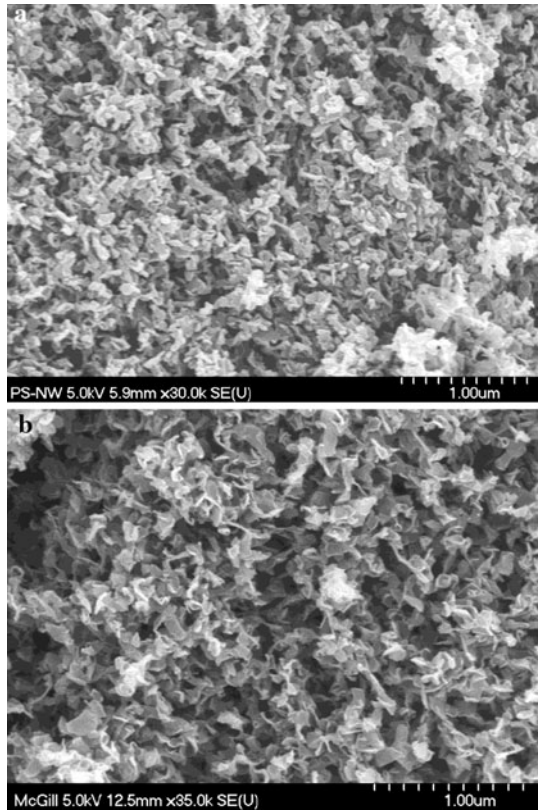
Carbon nanopowders were obtained by plasma decomposition of a carbon-containing feedstock. The material was produced using an inductively coupled thermal plasma (ICP) torch system of 35 kW using methane as a carbon precursor at various flow rates.

The induction plasma torch is a TEKNA PL-35 model, which is essentially composed of a copper coil of several turns wrapping a confinement tube inside which the induction plasma is generated. The plasma jet generated provides high temperatures (5,000–10,000 K) and high enthalpies (10^3 – 10^5 kJ/kg), depending on the species present in the system.² The injection probe is inserted into the torch in the axial position, the tip of the probe reaching the coil area of the torch body below the first coil turn, allowing the injection of the carbon source in the core of the plasma. Three gas streams are necessary for the operation of the ICP torch: central, sheath and carrier gas. The gas used for each of these streams was argon.

The ICP torch is attached to a conical water cooled reactor having 50 cm in length and a full angle of expansion of 14° (7° half angle) as presented in Fig. 1. Such geometry provides a gradual gas expansion from the torch to the reactor minimizing both recirculation areas and sudden quenching of the gas [15, 16]. A 4 mm annular gap between the

² Induction Plasma Torch PL-35 and PL-50, Operation and Service Manual. Sherbrook: Tekna Plasma Systems, Inc., 2004.

Fig. 2 SEM image of carbon nano-flakes obtained at: **a** 55.2 kPa and **b** 89.6 kPa



conical section of the reactor and the bottom collection plate is used for the gas outlet. An annular manifold around this outlet collects the exit gases which exit through a single outlet in the manifold. A higher pressure drop is maintained across the annular gap in comparison to the pressure drop in the manifold, ensuring in this way a radial outlet flow pattern of the gases from the collection plate. This geometry also provides a symmetric flow pattern within the reactor chamber above the collection plate and a stagnation point flow geometry on the plate itself [15].

The methane was injected using flow rates of 0.5, 1 and 5 slpm (measured at 294.5 K, 101.4 kPa). In some experiments nitrogen was also introduced along with the carbon source using flow rates of 0.1 and 0.2 slpm. The methane injection time varies between 5 and 32 min. In the experiments presented here, the reactor power is kept constant at about 20 kW plate power and two reactor pressures were used: 55.2 and 89.6 kPa.

Results and Discussions

Powders Produced Without Nitrogen Addition

The produced powders collected from different parts of the conical reactor show a uniform morphology [16], which was analyzed using scanning and transmission electron microscopy (SEM and TEM). The particles show a flake-like morphology (Figs. 2a,b and 3a,c)

hereafter called “carbon nano-flakes”, with typical dimensions of approximately 100 nm long, 50 nm wide and 5 nm thick. Close observation of the TEM micrograph (Fig. 3b,d) show the graphitic planes in the cross section with a stacking of between 6 and 16 planes in the powders observed. Similar CB structures were previously produced by DC thermal plasma system [17] and non-thermal plasma process [18].

The surface area of the powders as determined by the Brunauer Emmett Teller (BET) technique varied between 119 and 345 m²/g. The lower values were obtained for the samples in which the presence of organic volatile compounds was observed. It is believed that such organic compounds act as a glue causing the agglomeration of the carbon nano-flakes, and results in a decrease in the value of the specific surface area [16].

Raman spectroscopy was used to assess the degree of crystallinity of the produced materials. The Raman spectra presented in Fig. 4 were obtained using an incident laser wavelength of 514 nm and a grating of 1,800 lines/mm. All the spectra show distinct G

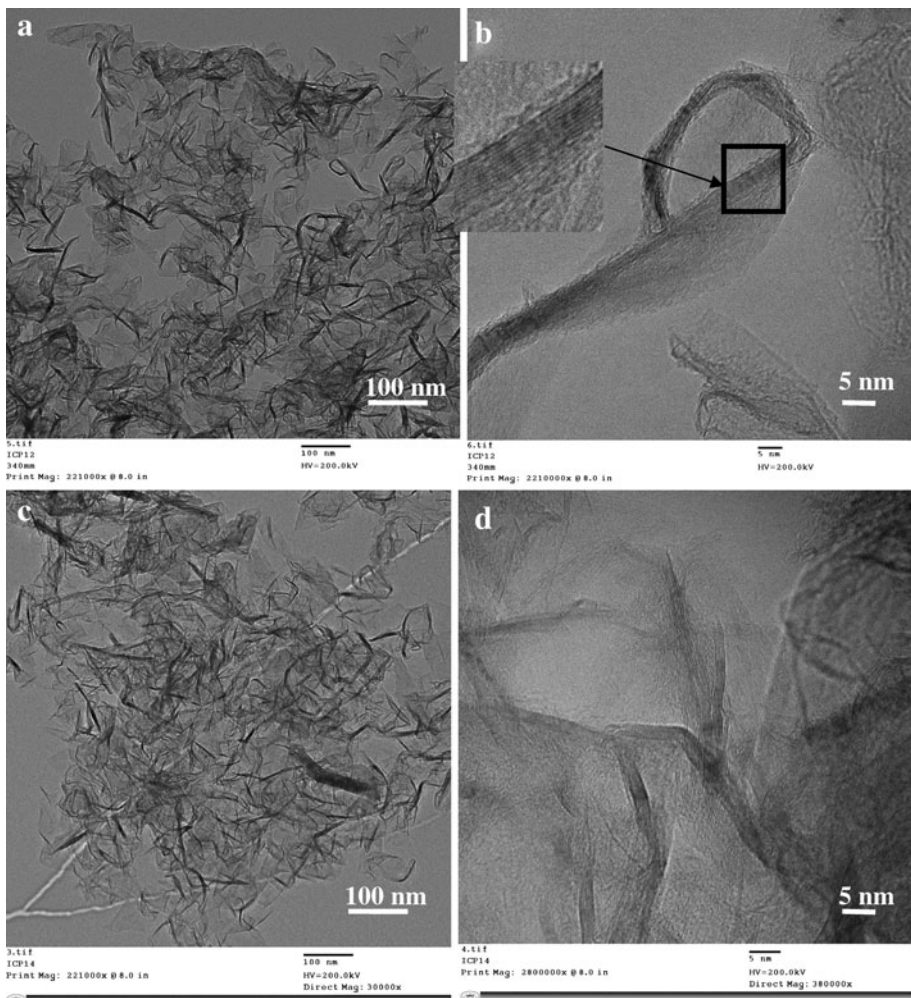
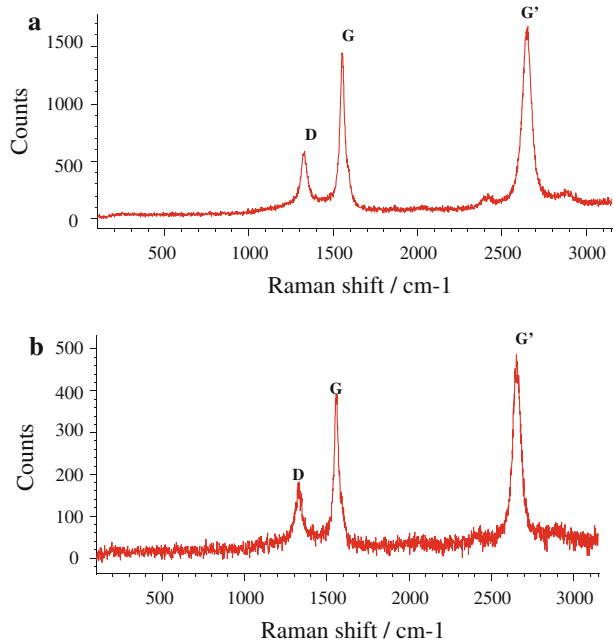


Fig. 3 TEM images of carbon nano-flakes obtained at: **a** and **b** 55.2 kPa, **c** and **d** 89.6 kPa

Fig. 4 Raman spectra of carbon nano-flakes produced at: **a** 55.2 kPa and **b** 89.6 kPa showing distinctive D and G primary bands and G' secondary band



band at $1,577\text{ cm}^{-1}$ and a D band at $1,345\text{ cm}^{-1}$, both being characteristic of graphitic materials, plus also the G' band at $2,697\text{ cm}^{-1}$. Analysis of the Raman spectra of natural graphite reveals a sharp and intense G band while the G' band is broader and less intense. The G' band changes in intensity and shape for carbon powders having a crystalline morphology composed of a small number of graphene layers (1–5 layers), becoming a single sharp and intense peak, more intense than the G band [19]. The powders produced in the present experiment show that the G' band is only slightly more intense than the G band. This seems to correlate with our powders being composed of graphene layers with a stacking of more than 5 layers.

The nano-flakes are composed of crystalline planes having an in-plane length (L_a) equal to 9.2 nm evaluated using the Raman-based method developed by Larouche and Stansfield [20]. This value is much higher than for other nanostructured carbon materials [20].

An assessment of the purity of the product can also be made from Raman spectra by using the relative ratios of the Raman peaks. The most suitable Raman ratio to use is the $I_{G'}/I_D$ ratio since the G' band results from a two-phonon process and its intensity decreases as the sample becomes less ordered because the impurities present in the sample does not allow the coupling effect necessary for the two-phonon process. By analyzing the Raman spectra obtained for the nano-flake powders, the calculated $I_{G'}/I_D$ ratio is around 2.5, which corresponds to a fully crystalline sample [21].

The X-Ray Diffraction (XRD) pattern shown in Fig. 5 is representative of powders obtained at 55.2 and 89.6 kPa. All the diffraction patterns show a crystalline structure. Comparing this with the diffraction pattern of natural graphite, one identifies the peaks around 2θ angles of 25° , 42° , 72° and 88° to be characteristic of a graphitic structure. The peaks around 2θ angles of 25° and 88° are reflections of the 002 and 006 diffraction lines, which are an indication of the graphite layers structure of the nano-flakes. The peaks around 2θ angles of 42° and 72° are reflections of the 100 and 104 diffraction lines and are assigned to the hexagonal symmetry of the graphene plane [22].

Fig. 5 Typical XRD diffraction pattern of carbon nano-flakes showing a crystalline structure

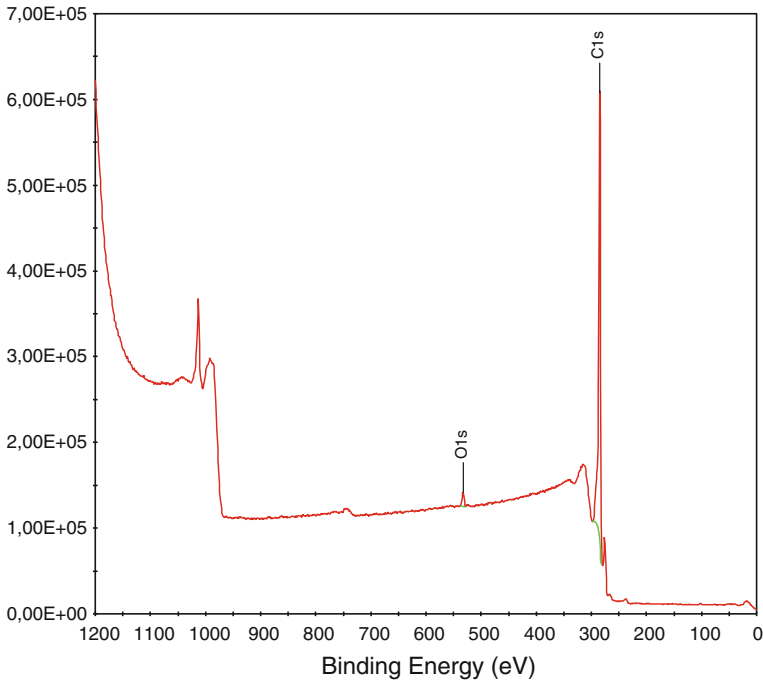
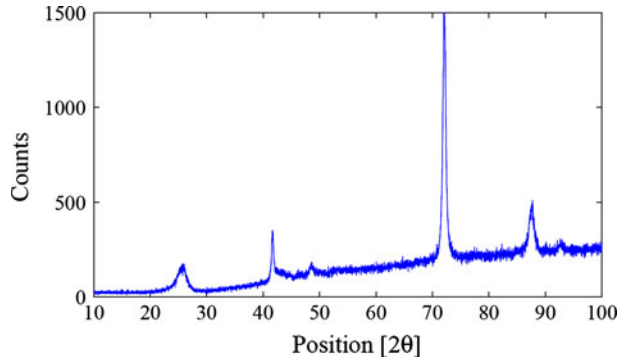


Fig. 6 XPS spectrum of carbon-nano flakes produced without nitrogen addition

The X-Ray Photoelectron Spectroscopy (XPS) results shown in Fig. 6 reveal the presence of two characteristic peaks: one C1s (carbon) peak at 284.9 eV and an O1s (oxygen) peak at 532.6 eV. These results show a high purity of the samples. The oxygen presence is due to exposure of samples to the ambient air. In these samples no nitrogen peak is observed as these experiments were performed without any addition of nitrogen to the plasma gas.

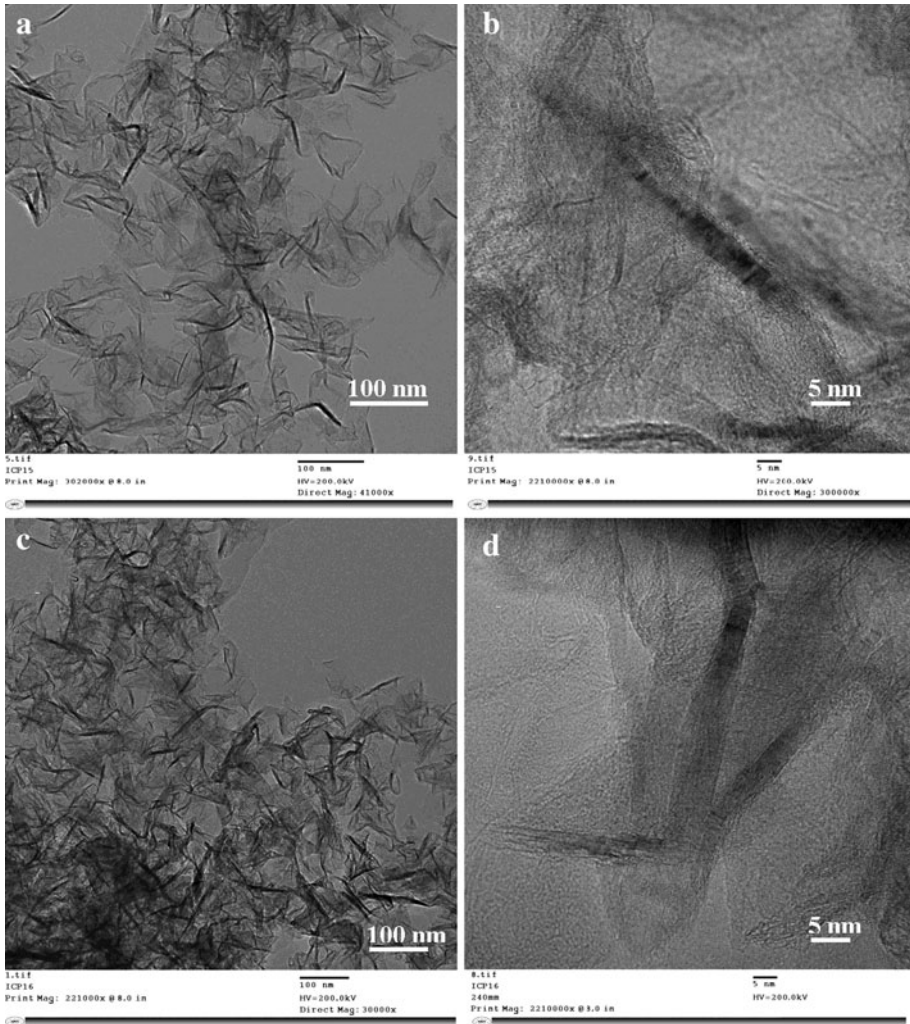


Fig. 7 TEM images of carbon nano-flakes obtained at: **a** and **b** 55.2 kPa, **c** and **d** 89.6 kPa and with nitrogen addition

Powders Produced with Nitrogen Addition

The TEM images shown in Fig. 7a,c reveal the same flake-like morphology of particles as in the case of the material produced without nitrogen addition. Close examination of TEM images (Fig. 7b,d) show a stacking with the same number of graphene planes (6–16) as in the case of powders produced without nitrogen addition. It can be concluded that the addition of nitrogen along with methane during the production process does not affect the morphology of the material.

Raman spectroscopy was used again to assess the crystallinity of the samples produced with the addition of nitrogen. No change was observed in the shape of the Raman spectra

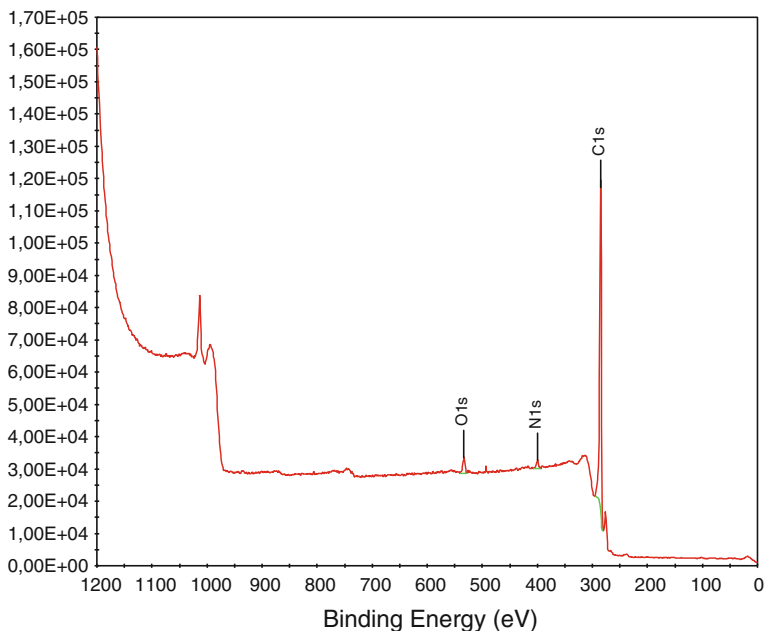


Fig. 8 XPS spectrum of carbon-nano flakes produced with nitrogen addition

of these samples if compared with the powders produced with no nitrogen addition (see Fig. 4). We observe again the presence of the distinct G band at $1,577\text{ cm}^{-1}$, D band at $1,345\text{ cm}^{-1}$ and G' band at $2,697\text{ cm}^{-1}$, all characteristic of graphitic materials. This is again an indication that the nano-flake morphology of the powders was not affected by the addition of nitrogen.

The XPS spectrum presented in Fig. 8 reveals the presence of the same two characteristic peaks observed in Fig. 6: one C1s (carbon) peak at 284.6 eV and an O1s (oxygen) peak at 532.2 eV, but also observed is the presence of a small N1s (nitrogen) peak at 398.8 eV. These results show again a high purity of samples. High resolution analysis of the N1s peak presented in Fig. 9 and the deconvolution of this peak shows that there are two types of N-bonding present: pyridinic type (peaks at 398.8 and 399.9 eV) and aliphatic type (peak at 410.1 eV).³ The amount of nitrogen incorporated into the desired pyridinic type structure is around $0.7 \pm 0.3\text{ at.}\%$, however the total amount measured in the samples was up to $2 \pm 1\text{ at.}\%$. The difference is nitrogen incorporated via the aliphatic type of N-bonding, most probably in a volatile organic compound. Further analysis on the solid carbon samples using thermal extraction techniques and GC–MS were made in various operating conditions of the reactor, these being presented in a separate publication. The main results for the samples produced using conditions of Fig. 7 indicate again a high purity of the samples.

³ National Institute of Standards and Technology (NIST), X-Ray Photoelectron Spectroscopy Database Version 3.5, www.nist.gov.

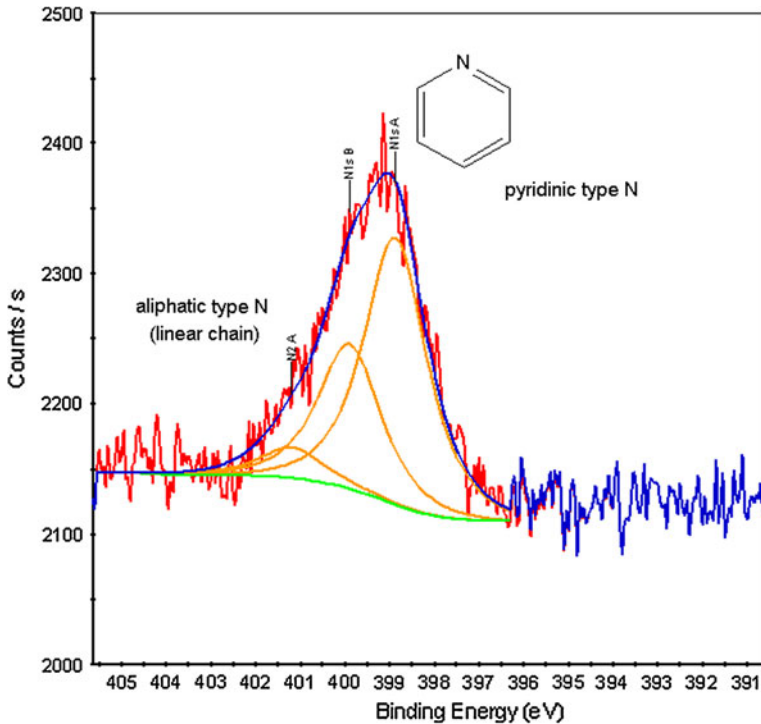


Fig. 9 XPS high resolution nitrogen peak (red line represents recorded data; blue line is the summation of deconvoluted peaks) showing two types of N-bonding: pyridinic type (N1sA peaks at 398.87 eV and N1sB peak at 399.90 eV) and aliphatic type (N2sA peak at 401.18 eV)

Conclusions

The present paper presents carbon nano-flakes produced using methane as a carbon precursor with or without the addition of nitrogen during the production process in an ICP thermal system. The uniform flow pattern achieved in the conical reactor enables a good control of the thermal history of the gas and solid particles in the conical reactor and promotes the formation of a clean product with a uniform morphology. It is showed that the addition of nitrogen did not affect the morphology of the powders. Up to 1.98 at.% of nitrogen is incorporated in the crystalline carbon powders, from which about 0.69 at.% is in the form of a pyridinic type of N-bonding. Such type of bonding is desired for the creation of active sites in a catalyst material for PEM fuel cells.

Acknowledgments The financial contributions of the Natural Sciences and Engineering Council of Canada, FQNR and General Motors Canada are gratefully acknowledged.

References

1. Donnet J-P, Voet A (1976) Carbon black. Physics, chemistry, and elastomer reinforcement. Marcel Dekker Inc, USA
2. Fabry F, Flamant G, Fulcheri L (2001) Carbon black processing by thermal plasma. Analysis of the particle formation mechanism. Chem Eng Sci 56:2123–2132

3. Girshick SL, Chiu CP, McMurphy PH (1988) Modelling particles formation and growth in a plasma synthesis reactor. *Plasma Chem Plasma Process* 8:145–157
4. Girshick SL, Chiu CP (1989) Homogeneous nucleation of particles from the vapor phase in thermal plasma synthesis. *Plasma Chem Plasma Process* 9:355–369
5. Fulcheri L, Schwob Y, Flamant G (1997) Comparison between new carbon nanostructured produced by plasma with industrial carbon black grades. *J Phys III France* 7:491–503
6. Juan L, Fangfang H, Yiwen L, Yongxiang Y, Xiaoyan D, Liao X (2003) A new grade carbon black produced by thermal plasma process. *Plasma Sci Technol* 5:1815–1819
7. Kim KS, Seo JH, Nam JS, Ju WT, Hong SH (2005) Production of hydrogen and carbon black by methane decomposition using DC-RF hybrid thermal plasmas. *IEEE Trans Plasma Sci* 33:813–823
8. Antolini E, Salgado JRC, Giz MJ, Gonzales ER (2005) Effects of geometric and electronic factors on ORR activity of carbon supported Pt-Co electrocatalysts in PEM fuel cells. *Int J hydrogen Energy* 30:1213–1220
9. Litster S, McLean G (2004) PEM fuel cell electrodes. *J Power Sour* 130:61–76
10. Barbir F (2005) PEM fuel cells. Theory and practice. Elsevier Inc, USA
11. Médard C, Lefevre M, Dodelet J-P, Jaouen F, Lindbergh G (2006) Oxygen reduction by Fe-based catalysts in PEM fuel cells conditions: activity and selectivity of the catalysts obtained with two Fe precursors and various carbon supports. *Electrochim Acta* 51:3202–3213
12. Lefevre M, Dodelet JP (2000) O₂ reduction in PEM fuel cells: activity and active site structural information for catalysts obtained by the pyrolysis at high temperature of Fe precursors. *J Phys Chem B* 104:11238–11247
13. Jaouen F, Lefevre M, Dodelet JP, Cai M (2006) Heat-treated Fe/N/C catalysts for O₂ electroreduction: are active sites hosted in micropores? *J Phys Chem* 110:5553–5558
14. Lee K, Zhan L, Zhan J (2008) PEM fuel cell electrocatalysts and catalyst layers: fundamentals and applications. Springer-Verlag London Limited, London
15. Castillo IA, Munz RJ (2007) New in situ sampling and new in situ sampling and analysis of the production of CeO₂ powders from liquid precursors using a novel wet collection system in a rf inductively coupled thermal plasma reactor. Part I: reactor system and sampling probe. *Plasma Chem Plasma Process* 27:737–759
16. Pristavita R, Mendoza-Gonzales NY, Meunier JL, Berk D (2010) Carbon blacks produced by thermal plasma: the influence of the reactor geometry on the product morphology. *Plasma Chem Plasma Process* 30:267–279
17. Li N, Wang Z, Zhao K, Shi Z, Gu Z, Xu S (2009) Large scale synthesis of N-doped multi-layered graphere sheets by arc-discharge method. *Carbon* 48:255–259
18. Moreno-Couranjou M, Monthieux M, Gonzalez-Aguilar J, Fulcheri L (2009) A non-thermal plasma process for the gas phase synthesis of carbon nanoparticles. *Carbon* 47:2310–2321
19. Ferrari AC, Meyer JC, Scardaci V, Casiraghi C, Lazzeri M, Mauri F, Jiand D, Novoselov KS, Roth S, Geim AK (2006) Raman spectrum of graphene and graphene layers. *Phys Rev Lett* 97:187401
20. Larouche N, Stansfield BL (2010) Classifying nanostructured carbons using graphitic indices derived from Raman spectra. *Carbon* 48:620
21. DiLeo R, Landi BL, Raffaele RP (2007) Purity assessment of multiwalled carbon nanotubes by Raman spectroscopy. *J Appl Phys* 101:064307
22. Inagaki M (2000) New carbons. Control of structure and functions. Elsevier Science Ltd, UK